2014

Cosmogenic 3He and 21Ne surface exposure dating of young basalts from Southern Mendoza, Argentina

Venera R. Espanon
University of Wollongong, vre981@uowmail.edu.au

Masahiko Honda
Australian National University, Masahiko.Honda@anu.edu.au

Allan R. Chivas
University of Wollongong, toschi@uow.edu.au

Publication Details

Espanon, V. R., Honda, M. & Chivas, A. R. (2014). Cosmogenic 3He and 21Ne surface exposure dating of young basalts from Southern Mendoza, Argentina. Quaternary Geochronology, 19 76-86.

Cosmogenic 3He and 21Ne surface exposure dating of young basalts from Southern Mendoza, Argentina

Abstract
Southern Mendoza, Argentina, is characterised by abundant Pleistocene to Holocene volcanism associated with back-arc magmatism, influenced by the subducting Nazca plate. Age determinations in this volcanic area have been improved during the last 5 years. However, there are some volcanic features especially in the Payunia Volcanic Field (PVF) which suggest fairly recent eruptions and which have not been chronologically determined. Recent studies on the Llancanelo Volcanic Field (LLVF) and PVF have determined volcanic activity mainly using K-Ar and 40Ar/39Ar as well as cosmogenic 3He. However, K-Ar and 40Ar/39Ar fail to produce reliable ages in Holocene basaltic flows. To better constrain the younger volcanic activity in the LLVF and especially in the PVF, surface exposure dating using cosmogenic 3He and 21Ne was applied to five volcanic features. By applying this method, 3He and 21Ne ages ranging from late Pleistocene to mid Holocene were obtained for basalts from the area of Los Volcanes, from the PVF. The youngest age acquired is significant as it supports previous evidence for mid Holocene volcanic activity in the PVF and constitutes the first noble gas cosmogenic surface exposure age obtained from a basaltic bomb. This paper illustrates the advantages of using two nuclides (3He and 21Ne) for cosmic-ray exposure ages in the study of recent volcanic eruptions. The results in the present study indicate that the PVF was active in the last 5 ka.

Keywords
mendoza, southern, basalts, young, argentina, dating, cosmogenic, exposure, 3he, surface, 21ne, GeoQuest

Disciplines
Medicine and Health Sciences | Social and Behavioral Sciences

Publication Details
Espanon, V. R., Honda, M. & Chivas, A. R. (2014). Cosmogenic 3He and 21Ne surface exposure dating of young basalts from Southern Mendoza, Argentina. Quaternary Geochronology, 19 76-86.

Cosmogenic ^{3}He and ^{21}Ne surface exposure dating of young basalts from southern Mendoza, Argentina.

Venera R. Espanon [a*], Masahiko Honda[b], Allan R. Chivas[a]

[a] *GeoQuest Research Centre*, *School of Earth & Environmental Sciences, University of Wollongong, NSW 2522, Australia*

[b] *Research School of Earth Sciences, The Australian National University, Canberra, ACT 0200, Australia.*

Masahiko Honda: Masahiko.Honda@anu.edu.au

Allan R. Chivas: toschi@uow.edu.au

*Corresponding author. Tel.: +61 24221 5899; fax: +61 242214250

E-mail address: vre981@uowmail.edu.au

Abstract

Southern Mendoza, Argentina, is characterised by abundant Pleistocene to Holocene volcanism associated with back-arc magmatism, influenced by the subducting Nazca plate. Age determinations in this volcanic area have been improved during the last 5 years. However, there are some volcanic features especially in the Payunia Volcanic Field (PVF) which suggest fairly recent eruptions and which have not been chronologically determined. Recent studies on the Llancanelo Volcanic Field (LLVF) and PVF have determined volcanic activity mainly using K-Ar and $^{40}Ar/^{39}Ar$ as well as cosmogenic ^{3}He. However, K-Ar and $^{40}Ar/^{39}Ar$ fail to produce reliable ages in Holocene basaltic flows. To better constrain the younger volcanic activity in the LLVF and especially in the PVF, surface exposure dating using cosmogenic ^{3}He and ^{21}Ne was applied to five volcanic features. By applying this method, ^{3}He and ^{21}Ne ages ranging from late Pleistocene to mid Holocene were obtained for basalts from the area of Los Volcanes, from the PVF. The youngest age acquired is significant as it supports previous evidence for mid Holocene volcanic activity in the PVF and constitutes the first noble gas cosmogenic surface exposure age obtained from a basaltic bomb. This paper illustrates the advantages of using two nuclides (^{3}He and ^{21}Ne) for cosmic-ray exposure ages in the study of recent volcanic eruptions. The results in the present study indicate that the PVF was active in the last 5 ka.

Keywords: Surface exposure dating; cosmogenic ^{3}He & ^{21}Ne; olivine; Mendoza; Argentina.

1. Introduction

On Earth's surface, highly energetic cosmic rays interact with target elements such as O, Na, Mg, Si and Al in rocks or sediments and produce in-situ terrestrial cosmogenic nuclides (TCNs, e.g. ^{3}He) (Poreda and Cerling, 1992; Niedermann, 2002; Ivy-Ochs and Kober, 2008; Gillen et al., 2010). This principle has formed the basis for the rapid development of a diverse spectrum of surface exposure dating (SED) techniques over the past two decades and has presented new prospects for the dating of Quaternary lava flows (e.g. Marti and Craig, 1987; Gillen et al., 2010; Marchetti et al., 2013). The most commonly used and extensively studied noble gas nuclide for surface exposure dating is ^{3}He, which can be used to date surfaces as young as 3 ka due to its high production rate and low detection limit using a conventional mass spectrometer (Gosse and Phillips, 2001).

By contrast, only a few attempts to date volcanic rocks and lava flows have utilised cosmogenic ^{21}Ne. In addition, ^{21}Ne can be readily compared to ^{3}He as the two nuclides cover the largest useful age range of all TCNs, and cosmogenic ^{3}He and ^{21}Ne can potentially record extremely long exposure histories as the two nuclides are stable (Gosse and Phillips, 2001). The two cosmogenic noble gas nuclides can be measured together in a sample because they are simultaneously accumulated with a constant production ratio since eruption. Thus, the combined application of cosmogenic ^{3}He and ^{21}Ne is considered of great potential for SED of lava flows. In this context, Poreda and Cerling (1992) have determined the absolute production rate for cosmogenic ^{21}Ne in olivine and plagioclase on independently dated young basalts from Tabernacle Hill, Utah. Furthermore, Fenton et al. (2009) have assessed cosmogenic ^{3}He and ^{21}Ne production rates in olivine and pyroxene from the western

Grand Canyon, Arizona, USA, while Gillen et al. (2010) used cosmogenic ^{21}Ne exposure dating in young basaltic lava flows from the Newer Volcanic Province, Victoria, Australia. Schmitt et al. (2010) have used radiogenic ^{4}He in combination with U-Th to date La Virgen tephra from Baja California and relate the ages with mafic lava flows dated using cosmogenic ^{3}He and ^{21}Ne. In addition, Schimmelpfennig et al. (2011) cross-calibrated cosmogenic ^{3}He, ^{21}Ne and ^{36}Cl production in mafic minerals, considering the altitude-dependence of the production rate, from the Kilimanjaro volcano, Tanzania. These studies have provided valuable examples of successful applications of cosmogenic ^{21}Ne dating in Quaternary lava flows, thereby suggesting that it can be applied to date Holocene flows from Southern Mendoza.

In principle, cosmogenic noble gases can be used to date lava flows that erupted only several years ago. In practice, however, the lower limit of exposure dating is controlled mainly by the combination of production rate, which depends on the nuclide and the site location, as well as the analytical detection limit (Gosse and Phillips, 2001). Furthermore, cosmogenic ^{3}He can theoretically be used to determine much younger exposure ages with accuracy and precision (<15%) since cosmogenic ^{3}He has a lower detection limit (from 5 x 10^{4} to 10^{5} atoms g^{-1} in Quaternary basaltic lavas; Blard et al., 2006) and a higher production rate. Nevertheless, to our knowledge, combined cosmogenic ^{3}He and ^{21}Ne to determine SED have not been explored in Holocene basaltic flows. Attempting to use cosmogenic ^{3}He and ^{21}Ne simultaneously would provide additional confidence on calculated ages since both nuclides are stable, have similar geochemical characteristics and can be extracted simultaneously using the same mineral separate. It should be noted, however, that this approach will not be suitable to identify complex exposure histories.

Since the production rate of cosmogenic nuclides is dependent mainly on altitude as well as target-element concentrations, the terrain of interest must be at a relatively high altitude in order to be able to date young volcanic flows. In the Andino-Cuyana Basaltic Province (ACBP) in northern Patagonia, Argentina, a wide range of landforms attest to a dynamic volcanic history since the early Pleistocene, including numerous well-preserved lava flows, some of which are among the longest in the world (Pasquarè et al., 2008). Even though many of the available chronological data for past eruptive activity have mainly provided mid- to late Pleistocene ages (Quidelleur et al., 2009; Germa et al., 2010; Gudnason et al., 2012; Marchetti et al., 2013), much younger volcanic activity (i.e., less than 10 ka) in the ACBP has been inferred based on geomorphic analysis (Inbar and Risso, 2001a) and a recent cosmogenic ^{3}He age by Marchetti et al. (2013). The ACBP therefore provides an ideal setting for the application of surface exposure dating of young, late Pleistocene to Holocene basaltic rocks located at a mean elevation of 2000 m above sea level (masl). Accordingly, this paper specifically aims at (i) evaluating the reliability of cosmogenic ^{3}He and ^{21}Ne dating when applied to Holocene volcanic rocks, thereby (ii) testing a possible practical younger limit of ^{21}Ne surface exposure dating, as well as (iii) contributing to the general chronology the LLVF and PVF.

2. Geological Setting

The study area is located between 35°30’S and 36°30’S and 69°45’W and 69°W, in the western-central part of Argentina (Figure 1) about 100-200 km east of the main Andean Cordillera (Inbar and Risso, 2001b). The ACBP comprises an area of 15,900 km^{2}, which is divided into two volcanic fields: the Llancanelo Volcanic Field (LLVF) to

the north and the Payunia Volcanic Field (PVF) to the south (Bermúdez and Delpino, 1989).

The subducting Nazca plate has been steepening for the last 5 Ma, after a period of shallow or near-horizontal subduction during the Miocene (Kay et al., 2004). The back-arc volcanism of the ACBP was caused by a steepening of the subducting slab, which introduced hot asthenospheric upwelling associated with melting of hydrated mantle (Stern, 2004; Quidelleur et al., 2009; Germa et al., 2010). The ACBP is dominated by basaltic and basaltic-andesitic flows. However, localised intermediate to felsic flows, such as trachyte, rhyolite and ignimbrite are also evident in the area of Cerro Nevado and around the Payún Matrú caldera in the PVF. There are more than 800 basaltic cones in the area, mainly monogenetic and a few polygenetic, many of which are aligned along a major east-west trending fault, the Carbonilla Fault (Llambías et al., 2010).

The chronological evolution of the area follows the previously described division of the ACBP. The more northerly LLVF is older than the PVF and this has been demonstrated by radiometric dating mainly based on K-Ar and $^{40}Ar/^{39}Ar$ methods. A K-Ar age from the eastern part of the LLVF is 1.88 ± 0.03 Ma which corresponds to the Pleistocene Nevado Formation; this age is the oldest in the area (Quidelleur et al., 2009). Recently, Gudnason et al. (2012) produced two $^{40}Ar/^{39}Ar$ ages from the LLVF of 0.16 ± 0.07 Ma and 0.28 ± 0.02 Ma, showing that this volcanic field was also active in the late Pleistocene. Furthermore, within the PVF, the oldest extensive pahoehoe lavas were erupted to the east of Payún Matrú caldera with K-Ar ages ranging from 0.95 ± 0.50 Ma to 0.6 ± 0.1 Ma (Melchor and Casadío, 1999). In addition, dates from the Payún Matrú caldera show that it was active in the last 300

ka and it has been suggested that the caldera-forming eruption occurred between 168 ± 3 ka and 82 ± 1 ka (using K-Ar, Germa et al., 2010). One of the youngest determined ages is 7 ± 1 ka from to a trachyte flow inside the Payún Matrú caldera (Germa et al., 2010). The youngest basaltic flows are from the area of Los Volcanes (eastern part of the PVF) dated at <7 ka (Germa et al., 2010). Recently, Marchetti et al. (2013) determined ^{3}He surface exposure ages from the late Pleistocene Puente Formation from the western part of Los Volcanes ranging from 41-43 ka. They also dated one of the young basaltic flows from Los Volcanes, calculating its age to 0 - 2 ka. Accordingly, the PVF has the most voluminous and most recent volcanic activity compared with other back-arc volcanic fields in Patagonia.

The erosion rate plays an important role when determining surface exposure ages because if not taken into consideration it could result in underestimating the exposure age. In the investigated volcanic area, semi-arid conditions with annual precipitation around 200 mm prevail (Inbar and Risso, 2001a). Winters are cold and summers are hot, with winds predominantly from the north-west and west (Inbar and Risso, 2001b). Hence, the erosion rate in basaltic rocks is assumed to be minimal. In this context, Marchetti et al. (2013) have applied a 1 mm ka^{-1} erosion rate to determine the age of basaltic flows using cosmogenic ^{3}He, also suggesting a low erosion rate. In addition, the elevation of the two volcanic fields is critical as it determines the cosmic ray influx. The LLVF is located at a mean elevation of 1500 masl while the PVF is located at approximately 2300 masl.

3. Methods

3.1 Sample selection and preparation

Five basaltic samples (LL3, PY-4, PY-7, PY-8 and PY-9) were collected for cosmogenic ^{3}He and ^{21}Ne surface exposure dating in February 2010 from the Llancanelo and Payunia Volcanic Fields (Figure 2, Table 1). The exposure surface and orientation of the rock was recorded for each sample. Samples LL3, PY-8 and PY-9 were collected from the original surface of different lava flows, which is one of the requirements for surface exposure dating. Samples PY-4 and PY-7 are small basaltic bombs, and they were assumed to have their surfaces exposed since ejection from the volcano. The size of the bombs was 14 cm by 7 cm and 10cm by 6cm for samples PY-4 and PY-7, respectively (Figure 2b). The weight of the bombs was ~1 kg and ~0.9 kg respectively. Furthermore, due to the low precipitation rate, it is unlikely that the bombs were transported from their airfall impact sites. In addition, Hernando et al. (2012) indicated that the bombs are in-situ as they preserve their aerodynamic or irregular shape and have preserved a small crater under each bomb, generated by their impact. However, considering the 8 cm maximum thickness of the bombs, the production rate for a potentially rotated bomb would be approximately 7% lower than at the original upper surface of the bomb. For a maximum age of 10 ka, a 7% decrease in the production rate, considering the same latitude, elevation and scaling factor, would account for a 700-year difference which is within the overall errors of the dating method.

Surface exposure dating was performed using olivine, extracted from 0.9 to 4.5 kg of sampled whole rock. Olivine separates were acquired by crushing the upper 5 cm of the basaltic flows and by crushing a whole basaltic bomb from each of the two bomb fields. After crushing and sieving, grain sizes of 355-180 µm and 180-106 µm were isolated as they contained the largest proportion of olivine single grains. The samples were cleaned with ~10% HCl acid to eliminate carbonate and subsequently

ultrasonically washed with distilled water. The minerals of interest were magnetically separated using a Frantz Isodynamic magnetic separator. The olivine-rich portion was further purified using density separation. The heavy liquids used were sodium polytungstate and methylene iodide with a maximum density of 3.00 g cm^{-3} and >3.33 g cm^{-3}, respectively. The olivine separates contained minor impurities of pyroxene, hornblende and spinel mainly from inclusions in the olivine crystals or as composite grains. Each olivine sample was carefully examined under a binocular stereo microscope and the residual impurities were removed by handpicking. The Mg content of the final olivine separate was quantified using X-ray fluorescence analysis. For noble gas analysis, two aliquots from samples LL3 and PY-9 were analysed, aliquot #1 constitutes the finer grain-size portion (180-106 µm) while aliquot #2 constitutes the coarser grain size (355-180 µm). For sample PY-7, the two grain sizes were combined to increase the olivine yield while for samples PY-4 and PY-8 only the coarser fraction was used. For X-ray fluorescence analysis of olivine, a single aliquot was used from each sample. Furthermore 0.1 g of whole-rock sample and olivine separate were digested from each sample using a mixture of HF and HNO_3 to measure Li, Th and U using an Agilent 7500cs ICP-MS at the University of Wollongong.

3.2 Isotopic analyses

Approximately 1 - 3 g of each olivine separate was wrapped in tin foil and loaded into an all-metal sample holder above a resistively heated, double-vacuum tantalum furnace on-line to a VG5400 noble gas mass spectrometer at the Australian National University. Details of the methods used to obtain the noble gas results are found in the Appendix.

4. Production rate

Production-rate calibration field sites are mainly based in the Northern Hemisphere and scaling factors assume the same cosmic ray influx in both hemispheres. However, since the Earth's geomagnetic field is not a perfect dipole, using a calibration site with similar latitude and altitude for the northern hemisphere will not be an ideal approximation for southern Mendoza. Goehring et al. (2010) presented a compilation of global ^{3}He production rates from different parts of the world, using several scaling factors. The average ^{3}He production rate in olivine proposed by Goehring et al. (2010) ranges from 121 ± 11 to 137 ± 16 at g^{-1} a^{-1} using the Lal (1991) and Lifton et al. (2005) scaling factors, respectively. For the present study, the former ^{3}He production rate was chosen. In addition, the two available ^{21}Ne production rates (Poreda and Cerling, 1992; Fenton et al., 2009) also use Lal's scaling factor. Therefore, for consistency we have used Lal's scaling factor in the current investigation.

The ^{21}Ne production rate is not only dependent on the geographical location of the study areas but also on the Mg content of olivine (Poreda and Cerling, 1992). From the literature, two ^{21}Ne production rates are reported, 45 ± 4 at g^{-1} a^{-1} (Poreda and Cerling, 1992) and 49 at g^{-1} a^{-1} (Fenton et al., 2009) for Fo_{81}, indicating that the ages obtained using Fenton's production rate are 0.92 times lower than those obtained using the Poreda and Cerling (1992) production rate. Since the Poreda and Cerling (1992) production rate is within uncertainty of that determined by Fenton et al. (2009) and is commonly used in the literature, we also utilised the former in our investigation. Furthermore, it is important to note that there are not enough ^{21}Ne production rate sites around the world in order to characterise a global production

rate. For the current study, the ^{21}Ne production rate is based on a calibration site in the Northern Hemisphere, hence assuming the same cosmic ray influx in both hemispheres.

The forsterite (Fo) content was calculated based on the major-element analysis by X-ray fluorescence and assuming that all the Mg measured corresponds to olivine (Table 2). The olivine purity is estimated at greater than 90%. In the current study, the production rate presented by Poreda and Cerling (1992), of 45 ± 4 at g^{-1} a^{-1} is based on similar Fo content (Fo_{81}) as in the samples investigated here (Table 2).

The scaling factor is critical in determining the production rate for each sample studied. The most commonly used and simplest is that of Lal (1991), which takes into account altitude and latitude. Nevertheless one of the limitations of using Lal's scaling factor is that it does not account for atmospheric pressure anomalies, which could be critical considering the proximity of the volcanic fields to a major mountain range. However, based on previous records, the atmospheric pressure at San Rafael (250 km north of the ACBP) presents no anomalies, as the value is 1013.7 ± 1.7 HPa when normalised to sea level and averaged over the years 1971 to 2004 (Schimmelpfennig et al., 2011). Lal's scaling factor was chosen for the current investigation, considering its broad acceptance (Poreda and Cerling, 1992; Fenton et al., 2009; and Gillen et al., 2010), its simplicity, and for consistency between the scaling factor used for the production rates of ^{3}He and ^{21}Ne.

Shielding corrections were not necessary for these samples as they were taken from the original surface of the flows and it is not likely that vegetation, snow or other volcanic debris covered the flows. The two bombs were carefully sampled to be less than 8 cm in thickness and the two bomb fields are not likely covered by any of the

material mentioned above. However, the bomb field where sample PY-4 was collected is inclined (Figure 2c); therefore the shielding was calculated using the Cronus-Earth geometric shielding calculator. The shielding factor for this sample is estimated to be 0.994.

The calculated cosmogenic ^{3}He production rate ranges from 341 at g^{-1} a^{-1} in sample LL3 to 625 at g^{-1} a^{-1} in sample PY-4, whereas the ^{21}Ne production rate ranges from 119 at g^{-1} a^{-1} to 232 at g^{-1} a^{-1} in the same samples.

5. Results

The He and Ne isotopic measurements from the olivine separates are listed in Table 3. Helium obtained by step-heating demonstrates the major release of cosmogenic ^{3}He (hereafter referred to as ^{3}He*) from mafic and ultramafic mineral separates, such as olivines, is below ~900-1100°C, whereas only minor amounts of cosmogenic ^{21}Ne (hereafter referred to as ^{21}Ne*) are released from the same minerals at temperatures below 900°C (Staudacher and Allègre, 1993; Niedermann, 2002). Table 3 clearly illustrates that the majority of cosmogenic ^{3}He was released at the lower extraction temperatures while the majority of cosmogenic ^{21}Ne was released at the higher extraction temperatures. However, significant fractions of ^{3}He were also released at higher temperatures, with ^{3}He/^{4}He ratios exceeding a typical mantle value of 1×10^{-5}. In order to calculate the concentrations of ^{3}He* and ^{21}Ne* in a sample, the total gas abundances, extracted at 900°C, 1400°C and 1750°C were used.

The total ^{3}He/^{4}He ratios measured in the samples by step-heating experiments range from $1.19 \pm 0.15 \times 10^{-5}$ (PY-7) to $26.78 \pm 0.77 \times 10^{-5}$ (LL3#2) while the ^{4}He concentrations range from $4.513 \pm 0.044 \times 10^{-9}$ (LL3#2) to $45.04 \pm 0.12 \times 10^{-9}$ (PY-

9#1) cm^3STP/g. The vacuum crushing of samples LL3, PY-4, PY-8 and PY-9 did not yield detectable amounts of ^{3}He above the blank level, despite applying 500 strokes during crushing. For sample PY-7, $^3He/^4He$ was 5.8 ± 2.9 x 10^{-5}, which could be interpreted as a release of cosmogenic helium, resulting from already finely crushed material (cf. Blard et al., 2008).

The $^{21}Ne/^{20}Ne$ isotope ratios observed in the samples range from 0.002879 ± 0.000078 (PY-7) to 0.00776 ± 0.00038 (LL3#2) and ^{20}Ne concentrations range from 6.04 ± 0.14 x 10^{-11} (LL3#1) to 24.19 ± 0.28 x 10^{-11} (PY-9#1) cm^3STP/g (Table 3). Samples PY-7 and PY-8 show a near-atmospheric $^{21}Ne/^{20}Ne$ ratio of 0.00296 (Figure 3).

5.1 Cosmogenic ^{3}He and ^{21}Ne

To calculate the concentration of each cosmogenic nuclide, it is important to estimate contributions from non-cosmogenic He and Ne components (Niedermann, 2002). Possible sources of non-cosmogenic components are: (i) radiogenic ^{4}He produced in-situ from radioactive decay of U and Th, (ii) nucleogenic ^{3}He produced from $^6Li(n,\alpha)^3H(\beta^-)^3He$, and (iii) nucleogenic ^{21}Ne from $^{18}O(\alpha,n)^{21}Ne$ (Niedermann, 2002). Non-cosmogenic nuclides can also be incorporated in a sample as a trapped component, which could be atmospheric, mantle or crustal in origin. To determine the trapped component, a vacuum crushing analysis was conducted. In the following sections we will assess the contributions from non-cosmogenic He and Ne components.

5.2 In-situ produced radiogenic ^{4}He and nucleogenic ^{3}He and ^{21}Ne

Radiogenic ^{4}He was calculated (Table 4) based on the U and Th content in olivine separates and whole-rock basalt using the equations described by Blard and Farley (2008). The U contents in the whole rocks range from 0.47 ppm (LL3) to 1.25 ppm (PY-7) while the Th content ranges from 1.98 ppm (LL3) to 8.82 ppm (PY-8). The calculated radiogenic ^{4}He concentrations in samples PY-4 and PY-7 are negligible, as the contribution from radiogenic ^{4}He to the total measured ^{4}He is less than 0.5% (Table 4). In the case of samples PY-8, PY-9#1 and PY-9#2, the contribution from radiogenic ^{4}He is less than 5%, while sample LL3 (two aliquots) shows a considerable contribution from radiogenic ^{4}He (11 % in LL3#1 and 35% in LL3#2). The corresponding correction for radiogenic ^{4}He was made for all of the samples. In addition, the Li content was measured in both whole rocks and olivine separates (Table 4). The Li data were used in conjunction with major-element data (Table 2) to calculate the contribution from nucleogenic ^{3}He to total ^{3}He, using the equation described by Andrews (1985) assuming a maximum eruption age (Table 4). The maximum age assumption was based on previous publications (Germa et al., 2010; Gudnason et al., 2012) and on the geological map of the area. It is concluded that the in-situ produced nucleogenic ^{3}He is negligible as its maximum production is 140 at g^{-1} accumulated in 100 ka for sample LL3#1 and LL3#2. The in-situ produced nucleogenic ^{21}Ne concentrations were calculated for each of the samples using the radiogenic ^{4}He concentrations and the $^{21}Ne_{nucleogenic}/^{4}He_{radiogenic}$ production ratio of 4.5×10^{-8} (Yatsevich and Honda, 1997), ranging from 2,100 at g^{-1} in sample LL3 (both aliquots) to 91 at g^{-1} in sample PY-7 (Table 4), which are negligible compared to those of cosmogenic origin.

5.3 Trapped helium and neon

To calculate $^{3}He^{*}$ and $^{21}Ne^{*}$ it is important to examine the fractions of He and Ne from mantle components. Generally, mantle components are referred to as trapped components as they are mainly found in fluid inclusions that could be derived from the mantle, crust or atmosphere when the lava was extruded. During vacuum crushing experiments, cosmogenic ^{3}He could be released as suggested by Blard et al. (2008). They postulated that temperature-enhanced volume diffusion is one of the main mechanisms responsible for controlling the release of $^{3}He^{*}$ during crushing. The $^{3}He^{*}$ released by vacuum crushing can be larger than 20% of the total cosmogenic ^{3}He in fine grained phenocrysts (<10 µm) (Blard et al., 2008). However, there is no report of cosmogenic ^{21}Ne release during vacuum crushing.

In the present study, the gases released by vacuum crushing showed low abundances of ^{4}He with negligible ^{3}He. As a result, the vacuum crushing experiment did not provide information regarding a helium isotope composition in a trapped component. Consequently we examined several possibilities in order to characterise a helium isotope composition in a trapped component. One is to use the R/R_a value of 6.9 ± 0.7 reported by Hilton et al. (1993) from the Central and Southern Volcanic Zone of the main Andean arc. A second possibility is to use the R/R_a values of 7.31, 7.29 and 7.68 from the western part of the Payunia Volcanic Field reported by Marchetti et al. (2013). The latter ratios are from the same geological and geographical area and from the same age range as the samples in the present study. Accordingly, an average R/R_a value of 7.43 ± 0.18 ($^{3}He/^{4}He = 1.027 \times 10^{-5} \pm 2.477 \times 10^{-7}$) was used for the trapped component in Equation 1 below.

A near-atmospheric $^{21}Ne/^{20}Ne$ ratio has been observed during the vacuum crushing analysis, implying no significant release of mantle Ne or crustal Ne. The atmospheric

value for $^{21}Ne/^{20}Ne$ is used for subtracting a trapped Ne component in Equation 2. In addition, the $^{22}Ne/^{20}Ne$ ratios measured during fusion range from 0.1022 in sample PY-9#1 at a step heating temperature of 900°C to 0.1286 in sample LL3#1 at a step heating temperature of 1400°C, indicating that the olivine separates do not contain mantle-derived Ne (Figure 3). The $^{22}Ne/^{20}Ne$ ratios from fusion in all heating steps are higher than the air and mantle-derived ratios of 0.1020 and 0.0769, respectively. In Equations (1) and (2), the symbol (*) denotes cosmogenic, while the subscript "meas" indicates measured.

$$^{3}He^{*} = {}^{4}He_{meas} \times \{(^{3}He/^{4}He)_{meas} - (^{3}He/^{4}He)_{trapped}\} \quad \textbf{(1)}$$

$$^{21}Ne^{*} = {}^{20}Ne_{meas} \times \{(^{21}Ne/^{20}Ne)_{meas} - (^{21}Ne/^{20}Ne)_{air}\} \quad \textbf{(2)}$$

In Figure 3 the Ne isotope compositions of the total fraction obtained from each of the samples are plotted on the Ne three-isotope diagram. For comparison, mixing lines for cosmogenic, mantle and crustal Ne with atmospheric Ne, as well as the Ne isotope fractionation line of atmospheric Ne are plotted on the diagram. The Ne isotope compositions for repeated analyses of samples LL3 and PY-9 (designated as #1 and #2) show large variations. The Ne isotope compositions for samples LL3#1 and PY-9#1 lie on the cosmogenic Ne mixing line, whereas those for samples LL3#2 and PY-9#2 are above the line. The offset of Ne data for the samples could be interpreted as involvement of a third component, such as crustal Ne. However, based on total ^{4}He concentrations observed in the samples and the ratio of the production rate of nucleogenic $^{21}Ne^{*}$ to radiogenic ^{4}He in the crust (4.5×10^{-8}; Yatsevich and Honda, 1997), the maximum contributions from either of the components to the concentrations of the total excess $^{21}Ne^{*}$ in the samples is less than 1%, and therefore the involvement of a crustal Ne component can be

discounted. Furthermore, we can exclude any instrumental pressure-dependence problems or any isobaric interference as possible interferences were properly corrected (see Appendix). Another possible explanation for the discrepancy among duplicates of samples LL3 (LL3#2) and PY-9 (PY-9#2), could be related to variable Ne mass-discrimination factors of the instrument during the analytical session. Lastly, the discrepancy could be simply sample-dependent as the duplicates have a different (coarser) grain size than the first aliquot analysed and the sample size was considerably larger. It would be desirable to undertake additional analyses to investigate these suggestions. However, as all collected material had been already consumed, the data could not be further authenticated. Based on the fact that the Ne data for samples LL3#1 and PY-9#1 lie on the cosmogenic Ne mixing line, we rely on these data and do not utilise the Ne data for samples LL3#2 and PY-9#2 for the following discussion.

Cosmogenic ^{3}He and ^{21}Ne and the resulting ages are summarised in Table 5. The amounts of ^{21}Ne* in sample PY-8 are not well constrained as the measured ^{21}Ne/^{20}Ne ratios are close to the atmospheric value (Table 3). Consequently, the concentration of ^{21}Ne* in sample PY-8 and the corresponding calculated age will not be discussed as the uncertainty associated with that age is >100%. Similarly, for sample PY-7 the total ^{21}Ne/^{20}Ne ratio from fusion analysis is atmospheric within uncertainty (Table 3 and Figure 3); hence this sample does not contain a sufficient amount of cosmogenic ^{21}Ne to calculate an age.

6. Discussion

The ^{3}He/^{4}He ratios measured in the five samples were higher than the assigned mantle ^{3}He/^{4}He ratio of 7.43 ± 0.18 R/R_a used in the present study, and detectable

amounts of $^{3}He^{*}$ were calculated by subtracting the mantle He for all samples. In contrast, this was not the case for $^{21}Ne^{*}$, as atmospheric neon overwhelmed $^{21}Ne^{*}$ in the younger samples.

Excluding the data for samples LL3 #2 and PY-9 #2, the $^{21}Ne^{*}/^{3}He^{*}$ ratios range from 0.06 ± 0.17 to 0.24 ± 0.01 in samples PY-8 and LL3#1, respectively (Table 5). The lower value corresponds to one of the youngest samples (PY-8) and for which the amount of sample analysed was 5-fold smaller than the other samples analysed. In sample PY-7 the $^{21}Ne^{*}/^{3}He^{*}$ ratio was not calculated as no $^{21}Ne^{*}$ was detected. The high uncertainty associated with $^{21}Ne^{*}/^{3}He^{*}$ in sample PY-8 and the lack of $^{21}Ne^{*}$ in sample PY-7 indicate that the detected and calculated levels of $^{21}Ne^{*}$ and $^{3}He^{*}$ for these two samples are particularly low. Consequently, the calculated concentrations of $^{3}He^{*}$ and $^{21}Ne^{*}$, as well as the corresponding ages for samples PY-7 and PY-8 from the Santa Maria volcano have large uncertainties. However, the low cosmogenic nuclide concentrations, in association with field observations, imply that this volcano is very young and may constitute one of the latest eruptions in the PVF before the current dormancy. As a result of the low cosmogenic helium and neon concentrations it can be estimated that these two samples are close to the practical younger limit of surface exposure dating utilising $^{3}He^{*}$ and $^{21}Ne^{*}$.

The $^{21}Ne^{*}/^{3}He^{*}$ ratios from samples LL3#1, PY-4 and PY-9#1 are listed in Table 5. The $^{21}Ne^{*}/^{3}He^{*}$ ratios are lower than the calculated $P^{21}Ne/P^{3}He$ (production rate ratio) values, and the cosmogenic $^{3}He^{*}$ ages are systematically older than the corresponding cosmogenic $^{21}Ne^{*}$ ages (Figure 4). The discrepancy could be related to improper subtraction of mantle He. As the He isotope compositions in trapped components were unable to be identified in the present study, we utilised the He

isotope composition of 7.43 ± 0.18 R/R_a, an averaged value previously determined in the same area (Marchetti et al., 2013), for the subtraction. However, the actual He isotope composition for each sample in the present study could be higher, and using the average value for the subtraction could result in older cosmogenic $^{3}He^*$ ages. In addition, it is important to note that the study area is located in a back-arc basin which according to the literature (Hilton et al. 2002 and references therein) may have a variable $^{3}He/^{4}He$ ratio ranging from well above the MORB value to well below MORB. Accordingly, $^{3}He/^{4}He$ ratios can vary considerably even within the same back-arc basin (Hilton et al. 2002 and references therein), therefore we could consider that the $^{3}He/^{4}He$ used for the current investigation is an approximation but may change from sample to sample. On this basis, in the present study we rely on cosmogenic $^{21}Ne^*$ ages, if available, rather than cosmogenic $^{3}He^*$ age, for the following discussion.

The cosmogenic surface exposure ages obtained from sample LL3 cannot be directly compared with earlier determined ages from other methods. The geographically nearest relevant sample to LL3 is 126191 from which Gudnason et al. (2012) obtained a $^{40}Ar/^{39}Ar$ date of 0.16 ± 0.07 Ma. The later sample is from a demonstrably older plateau lava (Cerro Jarilloso) that is 8 km west of LL3.

Sample PY-4 from Pampas Negras, PVF, constitutes the first volcanic bomb analysed by surface exposure dating using $^{3}He^*$ and $^{21}Ne^*$. For this sample, the ages produced using $^{3}He^*$ and $^{21}Ne^*$ do not agree at 1σ uncertainty (Figure 4). However, they both accord with a maximum K-Ar age (<7 ka) reported by Germa et al. (2010) from a basaltic flow (sample 88AB) located in the same area as PY-4. Hernando et al. (2012) used the date from Germa et al. (2010) to map the large

scoria and cone field (Figure 5) of the northern Pampas Negras as mid-Holocene in age. The 1:250,000 geological map of the region (Narciso, 2004) appropriately equates this field to the mid-Holocene Tromen Formation, although its type area is Volcán Tromen, some 100 km southwest of Pampas Negras.

The ^{21}Ne* surface exposure date from sample PY-9#1 derives from an older ropy-surfaced basaltic lava flow sourced from near the northwestern flank of Payún Matrú. This flow has not been dated previously, although a parallel northerly flow 6 km further to the east (Figure 5) has a broadly comparable K-Ar age of 28 ± 5 ka (sample 94AF of Germa et al., 2010)

Our results further reinforce the importance of careful characterisation of radiogenic ^{4}He, as in sample LL3, where the contribution of radiogenic ^{4}He to the total ^{4}He is quite high (Table 4). In addition, it is also shown that the precise determination of the helium trapped-component is critical to produce confident exposure ages. This study also shows that the PVF was active until at least the mid Holocene. Based on field observations, the age obtained (or inability to obtain an age) for the two youngest samples (basaltic bombs PY-4 and PY-7) may represent the latest stages of volcanic activity in the PVF.

This study demonstrates that the younger limit of surface exposure dating using ^{3}He* and ^{21}Ne* may be placed at approximately 5 ka, with current technology. Furthermore, it emphasizes the importance of using two nuclides to cross-compare results. The practical younger limit of the method has to be further studied, however, it is possible that with improved technologies (cf. Gillen et al., 2010), such as a multi-collector mass spectrometer or a “compressor ion source” (Baur, 1999), smaller quantities of noble gases might be detected with higher precision and less

uncertainty. The younger dating limit is variable and will depend not only on the technology used but also careful sample preparation and on the accuracy with which trapped components can be resolved.

7. Conclusion

This investigation demonstrates the advantages of using the paired in-situ produced cosmogenic noble gases ^{3}He and ^{21}Ne and shows that it is possible to date basalts as young as 5 ka. Nevertheless, the 5 ka younger age limit has to be taken cautiously as this is dependent, in this case, on high production rates resulting from the relatively high-elevation field sites and where the production rate is 5.2 times higher than for a similar sample at mid-latitude and at sea level. The age obtained for sample PY-4 using cosmogenic ^{21}Ne constitutes the youngest age obtained from the PVF with acceptable errors, not considering the age obtained using cosmogenic ^{3}He. Nevertheless, if we also accept the surface exposure age produced using cosmogenic ^{3}He, the previous statement would not change.

The Llancanelo and Payunia Volcanic fields are suggested as possible Southern Hemisphere cosmogenic calibration sites as they have a wide chronology ranging from ~1Ma to <10 ka. In summary, the cosmogenic ^{3}He and ^{21}Ne paired approach suggests that the Payunia Volcanic Field was active until approximately 5 ka and possibly to less than 3 ka, although the younger age estimations need to be further investigated.

Appendix.

1. Noble gas analyses

Helium and neon analyses were undertaken in the Noble Gas Laboratory at the Research School of Earth Sciences, Australian National University. The details of analytical procedure are essentially identical to those described in Gillen et al. (2010), and are briefly summarised below.

Gases were released from samples either by step-wise heating in a furnace, or by crushing under vacuum. The furnace consists of a tantalum crucible and connecting tubes. To prevent samples reacting with the tantalum crucible, samples were loaded into a disposable molybdenum liner inside the crucible. Approximately 1 - 3 g of each olivine separate was wrapped in tin foil and loaded into an all-metal sample holder above a resistively heated, double-vacuum tantalum furnace, and the noble gases were extracted by three heating steps for aliquot #1 (900°C, 1400°C and 1750°C) and two heating steps (900°C and 1750°C) for aliquot #2 in samples LL3 and PY-9 and the remaining analysed samples. Each sample was held at each heating temperature for 30 min. Prior to sample analysis, the Ta crucible and Mo liner were degassed at 1850°C for at least 2 h. After the blank measurement, a sample was dropped into the Ta crucible for analysis. Vacuum crushing analysis provides information on trapped He and Ne components in a sample. Trapped gases in fluid inclusions correspond to either mantle, crustal or atmospheric components, which need to be characterized in order to determine concentrations of cosmogenic nuclides. For this procedure, approximately 1 g of each sample was crushed under vacuum, using an air-actuated crushing apparatus comprising a stainless crusher vessel (Matsumoto et al., 2001). Each sample was crushed by 500 strokes. Blank

measurements were performed both for step-heating and crushing experiments before and after sample analyses.

Purification and separation of gases released from a sample are achieved by exposure to a series of Ti getters and two activated charcoal traps. The gas is first exposed to the Ti bulk getters, operated at 300°C, to remove the bulk of active species (most importantly nitrogen and oxygen). Subsequently, the gas is exposed to a SAES® getter operated at room temperature to absorb hydrogen, and a second SAES getter, operated at 250°C, to remove residual active species. Following this, a third SAES getter, operated at room temperature, removes any remaining active species, particularly hydrogen, in the sample. Samples were analysed using a VG5400 mass spectrometer equipped with a Faraday collector with a fixed resolution of 230 and a Daly multiplier collector with a fixed resolution of 600. The Faraday collector is used to measure ^{4}He and the Daly collector is used to measure ^{3}He and the isotopes of neon. The mass spectrometer operating conditions used throughout the period of analyses (July – September 2010) were: source accelerating voltage 4.5 kV; electron ionisation potential 75 V; trap current 200 µA; repeller voltage -3.4 V relative to the source chamber. Focus and beam centring conditions were optimised automatically to maximise beam intensity for each noble gas. The overall gain of the Daly collector and photomultiplier when operated at 10 kV and 960 V, respectively, was approximately 1 x 10^{6}. The detection limit for both ^{3}He and neon, based on noise from the Daly detector, was equivalent to ~ 2 x 10^{-14} cm^{3}STP.

2. Sensitivity and mass discrimination

Sensitivity and mass discrimination values were checked at regular intervals. These were achieved by analysing gas standards of known volume and isotopic

composition. Two noble gas pipettes, the HESJ and the Heavy Gas, are attached to the sample system. The Heavy Gas Pipette was prepared from air in Canberra, and active gases were removed by hot Ti-bulk getters. One aliquot of the Heavy Gas Pipette contains 2.3 x 10^{-9} cm^3STP of ^{20}Ne. Helium was calibrated using the HESJ Pipette (with $^3He/^4He$ = 2.89 x 10^{-5} (or 20.6 R/R_a); Matsuda et al., 2002), and one aliquot of it contains 4.0 x 10^{-7} cm^3STP of ^{4}He. These amounts are based on Boyles's law, using a Baratron manometer. The amount of Ar in the Heavy Gas Pipette was cross-checked by a ^{38}Ar spike used for the K-Ar dating at ANU (McDougall, personal communication). The Ar amounts agreed to within 1%. The amount of He in one aliquot of the HESJ Pipette was crosschecked against ^{4}He in the He standard prepared by Des Patterson which had been calibrated against the Caltech He standard (Patterson, personal communication). Sensitivities for ^{4}He and ^{20}Ne based on repeated analyses of the pipettes were 1.60 $\pm$ 0.02 x 10^{-5} and 6.16 $\pm$ 0.09 x 10^{-5} A/cm^3, respectively, using a 200 µA trap current. Mass discrimination factors are defined as the known isotopic ratio of the gas standards, divided by the measured ratio. Mass discrimination factors for helium and neon were 1.42 $\pm$ 0.03, which included the compensation of the Daly gain for ^{3}He; $^{21}Ne/^{20}Ne$: 1.0167 $\pm$ 0.006; and $^{22}Ne/^{20}Ne$: 1.039 $\pm$ 0.001. The dependence of sensitivity and mass discrimination on gas pressure in the mass spectrometer were examined by measurements of successively diluted aliquots of the gas pipettes. Both the sensitivity and mass discrimination of He and Ne is constant within experimental uncertainties over a pressure range during the present study. Uncertainties in sensitivities and mass discrimination factors are properly propagated to final results summarised in Table 3.

3. Neon isotope analysis

Corrections are typically required for mass interference of $^{40}Ar^{++}$ on ^{20}Ne; CH_2CO^{++} (double charged mass 42) on ^{21}Ne, and CO_2^{++} on ^{22}Ne. The ratios of double charged to single charged CO_2 and CH_2CO were estimated from background measurements on a static operation in the mass spectrometer in the absence of detectable Ne; values of 0.003 ± 0.0003 and $(1.5 \pm 0.15) \times 10^{-3}$ were estimated, respectively. The correction for double charged ^{40}Ar was estimated by increasing the amount of Ar added to the Ne fraction by warming the cryogenic charcoal to a slightly higher temperature than Ne release temperature (= 125 K), and the value of 0.199 ± 0.051 was estimated. Contributions of the $^{40}Ar^{++}$, CH_2CO^{++} and CO_2^{++} interferences on ^{20}Ne, ^{21}Ne and ^{22}Ne in samples during this study ranged 0.5 – 4.0 %, 0.03 – 0.1 % and 0.3 – 3.0 %, respectively.

4. Blanks

Following outgassing of the furnace at 1850°C, blanks were measured for 1400 and 1750°C heating experiments and for vacuum crushing. Regardless of the extraction methods or heating temperatures, blank amounts were $4 - 2 \times 10^{-10}$ cm^3STP for ^4He, $5 - 2 \times 10^{-14}$ cm^3STP for ^3He, and $4 - 2 \times 10^{-12}$ cm^3STP for ^{20}Ne. These blank amounts were subtracted from the total gases released during the experiments. For Ne, atmospheric Ne isotope compositions were used for blank subtractions.

Acknowledgements

We thank the park rangers in Llancanelo and Payunia Provincial Natural Reserve (Mendoza), Daniel Smith, Adriana Garcia (University of Wollongong), Sabina

D’Ambrosio (Universidad Nacional de La Plata, Argentina), Leandro Rojo (Museo de Ciencias Naturales de San Rafael) and Jorge Chielsa (Universidad Nacional de San Luis, Argentina) for their assistance during field work. Shane Paxton and Igor Yatsevich (Australian National University) helped purify some olivine samples. Constructive comments on the manuscript were made by Luke Gliganic. We would like to thank Dr Samuel Niedermann and an anonymous reviewer for their very constructive reviews that helped to improve the manuscript. The fieldwork component of this study was funded in part by grant PICT1311-06 from Agencia Nacional de Programación Científica y Tecnológica, Argentina, within which Chivas is a collaborator. Additional fieldwork for Espanon and Chivas was supported by a short-term mobility scholarship for field training in young geological processes from the then Department of Industry, Innovation, Science, Research and Tertiary Education of the Australian Government.

References

Andrews, J.N., 1985. The isotopic composition of radiogenic helium and its use to study groundwater movement in confined aquifers. Chemical Geology 49, 339–351.

Baur, H., 1999. A noble-gas mass spectrometer compressor source with two orders of magnitude improvement in sensitivity. Eos (Transactions, American Geophysical Union) 46, F1118.

Bermúdez, A., Delpino, D., 1989. La provincia basaltica Andino Cuyana (35-37°L.S.). Revista de la Asociación Geológica Argentina 40, 35-55.

Blard, P.-H., Pik, R., Lavé, J., Bourlès, D., Burnard, P.G., Yokochi, R., Marty, B. Trusdell, F., 2006. Cosmogenic ^{3}He production rates revisited from evidences of grain size dependent release of matrix-sited helium. Earth and Planetary Science Letters 247, 222-234.

Blard, P.-H.,Farley, K.A., 2008. The influence of radiogenic ^{4}He on cosmogenic ^{3}He determinations in volcanic olivine and pyroxene. Earth and Planetary Science Letters 276**,** 20-29.

Blard, P.-H., Puchol, N., Farley, K.A., 2008. Constraints on the loss of matrix-sited helium during vacuum crushing of mafic phenocrysts. Geochimica et Cosmochimica Acta 72, 3788-3803.

Fenton, C.R., Niedermann, S., Goethals, M.M., Schneider, B., Wijbrans, J., 2009. Evaluation of cosmogenic ^{3}He and ^{21}Ne production rates in olivine and pyroxene from two Pleistocene basalt flows, western Grand Canyon, AZ, USA. Quaternary Geochronology 4, 475-492.

Germa, A., Quidelleur, X., Gillot, P.Y., Tchilinguirian, P., 2010. Volcanic evolution of the back-arc Pleistocene Payun Matru volcanic field (Argentina). Journal of South American Earth Sciences 29, 717-730.

Gillen, D., Honda, M., Chivas, A.R., Yatsevich, I., Patterson, D.B., Carr, P.F., 2010. Cosmogenic ^{21}Ne exposure dating of young basaltic lava flows from the Newer Volcanic Province, Western Victoria, Australia. Quaternary Geochronology 5, 1-9.

Goehring, B.M., Kurz, M.D., Balco, G., Schaefer, J.M., Licciardi, J., Lifton, N., 2010. A reevaluation of in situ cosmogenic ^{3}He production rates. Quaternary Geochronology, 5, 410-418.

Gosse, J.C., Phillips, F.M., 2001. Terrestrial *in situ* cosmogenic nuclides: theory and application. Quaternary Science Reviews 20, 1475-1560.

Gudnason, J., Holm, P.M., Søager, N., Llambías, E.J., 2012. Geochronology of the late Pliocene to Recent volcanic activity in the Payenia back-arc volcanic province, Mendoza Argentina. Journal of South American Earth Sciences 37, 191-201.

Hernando, I.R., Llambías, E.J, González, P.D., Sato K., 2012. Volcanic stratigraphy and evidence of magma mixing in the Quaternary Payún Matrú volcano, Andean backarc in western Argentina. Andean Geology 39, 158-179.

Hilton, D.R., Fischer, T.P., Marty, B., 2002. Noble Gases and Volatile Recycling at Subduction Zones. In: Porcelli, D., Ballentine, C.J., Wieler, R. (Eds.), Noble Gases in Geochemistry and Cosmochemistry. Reviews in Mineralogy & Geochemistry. Mineralogical Society of America, Washington, DC, pp. 319–370.

Hilton D.R., Hammerschmidt, K, Teufel, S., Friedrichsen, H., 1993. Helium isotope characteristics of Andean geothermal fluids and lavas. Earth and Planetary Science Letters 120, 265-282.

Inbar, M., Risso, C., 2001a. A morphological and morphometric analysis of high density cinder cone volcanic field - Payun Matru, south-central Andes, Argentina. Zeitschrift für Geomorphologie N. F. 45, 321-343.

Inbar, M., Risso, C., 2001b. Holocene yardangs in volcanic terrains in the southern Andes, Argentina. Earth Surface Processes and Landforms 26, 657-666.

Ivy-Ochs, S., Kober, F., 2008. Surface exposure dating with cosmogenic nuclides. Eiszeitalter und Gegenwart 57, 179-209.

Kay, S.M., Gorring, M., Ramos, V. A., 2004. Magmatic sources, setting and causes of Eocene to Recent Patagonian plateau magmatism (36°S to 52°S latitude). Revista de la Asociación Geológica Argentina 59, 556-568.

Kennedy, B.M., Hiyagon, H., Reynolds, J.H., 1990. Crustal neon: a striking uniformity. Earth and Planetary Science Letters 98, 277-286.

Lal, D., 1991. Cosmic ray labeling of erosion surfaces: in situ nuclide production rates and erosion models. Earth and Planetary Science Letters 104, 424-439.

Licciardi, J.M., Kurz, M.D., Curtice, J.M., 2006. Cosmogenic ^{3}He production rates from Holocene lava flows in Iceland. Earth and Planetary Science Letters 246, 251-264.

Lifton, N., Bieber J.W., Clem, J.M., Duldig, M., Everson, P., Humble J.E., Pyleet R., 2005. Addressing solar modulation and long-term uncertainties in scaling secondary cosmic rays for in situ cosmogenic nuclide applications. Earth and Planetary Science Letters 239, 140-161

Llambías, E.J., Bertotto, G., Risso, C., Hernando, I., 2010. El volcanismo Cuaternario en el retroarco de Payenia: Una revisión. Revista de la Asociación Geológica Argentina 67, 278-300.

Marchetti, D., Hynek, S., Cerling, T., 2013. Cosmogenic ^{3}He exposure ages of basalt flows in the northwestern Payún Matru volcanic field, Mendoza Province, Argentina. Quaternary Geochronology (in press).

Marti, K., Craig, H., 1987. Cosmic-ray-produced neon and helium in the summit lavas of Maui. Nature 325, 335-337.

Matsuda, J., Matsumoto, T., Sumino, H., Nagao, K., Yamamoto, J., Miura, Y., Kaneoka, I., Takahata, N., Sano, Y., 2002. The ^{3}He/^{4}He ratio of the new internal He Standard of Japan (HESJ). Geochemical Journal 36, 191-195.

Matsumoto, T., Chen, Y., Matsuda, J., 2001. Concomitant occurrence of primordial and recycled noble gases in the Earth's mantle. Earth and Planetary Science Letters 185, 35-47.

Matsumoto, T., Honda, M., McDougall, I., Yatsevich, I., O'Reilly S. Y., 2004. Isotope fractionation of neon during stepheating extraction?: A comment on "Re-interpretation of the existence of a primitive plume under Australia based on neon isotope fractionation during step heating" by Gautheron and Moreira (2003). Terra Nova 161, 23-24.

Melchor, R.N., Casadío, S., 1999. Boletín 295 Hoja Geológica 3766-III, La Reforma, Provincia de La Pampa, Servicio Geológico Minero Argentino, Buenos Aires, 73 pp.

Narciso, V., 2004. Boletín 253 Hoja Geológica 3769-I, Barrancas, Servicio Geológico Minero Argentino, Buenos Aires, 68 pp.

Niedermann, S., 2002. Cosmic-Ray-Produced Noble Gases in Terrestrial Rocks: Dating Tools for Surface Processes. In: Porcelli, D., Ballentine, C.J., Wieler, R. (Eds.), Noble Gases in Geochemistry and Cosmochemistry. Reviews in Mineralogy & Geochemistry. Mineralogical Society of America, Washington, DC, pp. 731–784.

Pasquarè, G., Bistacchi, A., Francalanci, L., Bertotto, G., Boari, E., Massironi, M., Rossotti, A., 2008. Very long pahoehoe inflated basaltic lava flows in the Payenia Volcanic Province (Mendoza and La Pampa, Argentina). Revista de la Asociación Geológica Argentina 63, 131-149.

Poreda, R., Cerling, T., 1992. Cosmogenic neon in recent lavas from the western United States. Geophysical Research Letters 19, 1863-1866.

Quidelleur, X., Carlut, J., Tchilinguirian, P., Germa, A., Gillot, P.Y., 2009. Paleomagnetic directions from mid-latitude sites in the southern hemisphere (Argentina): Contribution to time averaged field models. Physics of the Earth and Planetary Interiors 172, 199-209.

Sarda, P., Staudacher, T., Allègre, C.J., 1988. Neon isotopes in submarine basalts. Earth and Planetary Science Letters 91, 73-88

Schäfer, J.M., Ivy-Ochs, S., Wieler, R., Leya, I., Baur, H., Denton, G.H., Schlüchter, C., 1999. Cosmogenic noble gas studies in the oldest landscape on earth: surface exposure ages of the Dry Valleys, Antarctica. Earth and Planetary Science Letters 167**,** 214-226.

Schimmelpfennig, I., Benedetti, L., Garreta, V., Pik, R., Blard, P.-H., Burnard, P., Bourlès, D., Finkel, R., Ammon, K., Dunai, T., 2011. Calibration of cosmogenic ^{36}Cl production rates from Ca and K spallation in lava flows from Mt. Etna (38^{o}N, Italy) and Payun Matru (36^{o}S, Argentina). Geochimica et Cosmochimica Acta 75, 2611-2632.

Schimmelpfennig, I., Williams, A., Pik, R., Burnard, P., Niedermann, S., Finkel, R., Schneider, B., Benedetti, L., 2011. Inter-comparison of cosmogenic in-situ ^{3}He, ^{21}Ne and ^{36}Cl at low latitude along an altitude transect on the SE slope of Kilimanjaro volcano (3°S, Tanzania). Quaternary Geochronology 6**,** 425-436.

Schmitt A., Stockli D., Niedermann S., Lovera O., Hausback B., 2010. Eruption ages of Las Tres Vírgenes volcano (Baja California): A tale of two helium isotopes. Quaternary Geochronology 5**,** 503-511.

Staudacher, T., Allègre, C.J., 1993. The cosmic ray produced ^{3}He/^{21}Ne ratio in ultramafic rocks. Geophysical Research Letters 20, 1075-1078.

Stern, C.R., 2004. Active Andean volcanism: its geologic and tectonic setting. Revista Geológica de Chile 31, 161-206.

Vermeesch, P., 2007. CosmoCalc: An Excel add-in for cosmogenic nuclide calculation. Geochemistry, Geophysics, Geosystems 8(8): Q08003.doi:08010.01029/02006GC001530.

Yatsevich, I., Honda, M., 1997. Production of nucleogenic neon in the Earth from natural radioactive decay. Journal of Geophysical Research 102, 10291-10298.

Figure Captions

Fig 1: Geographical setting of the Llancanelo and Payunia volcanic fields, western Argentina. The white dots indicate sampling locations. The white line indicates the Carbonilla Fault.

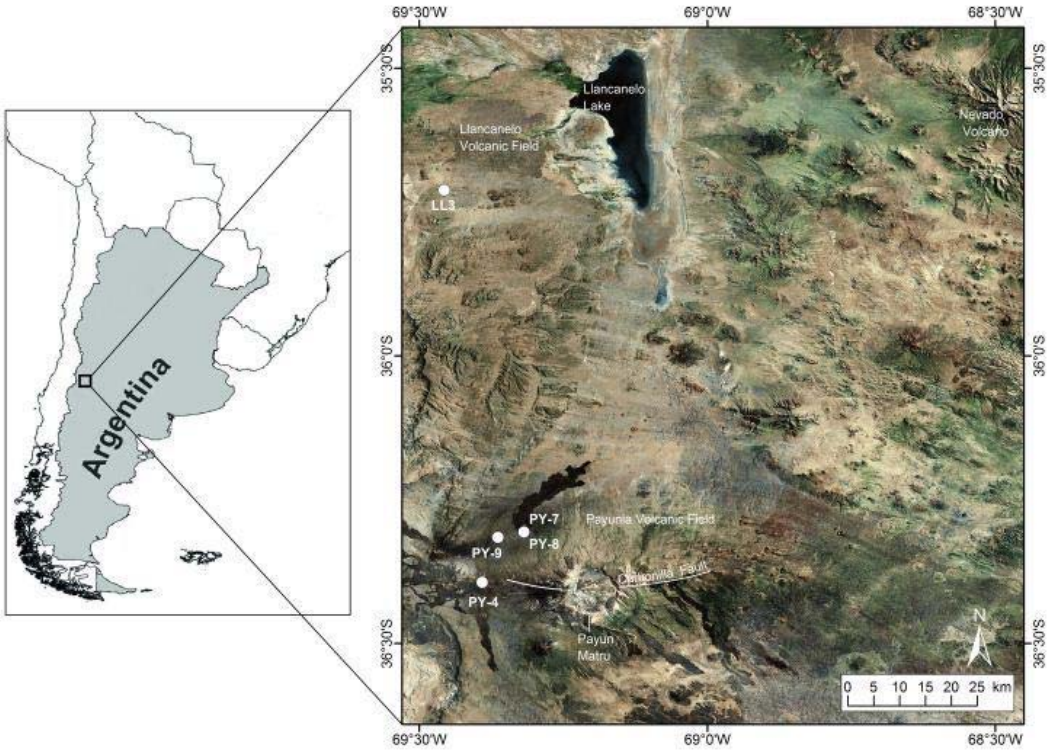

Fig 2: Field sites in the Llancanelo (LLVF) and Payunia Volcanic (PVF) Fields, Mendoza Province. a) Sample LL3 from the upper part of a steeply dipping basaltic tumulus, LLVF; upper geological hammer (circled) for scale. b) Basaltic bombs (PY- 4) from Pampas Negras, Los Volcanes, PVF (circle indicates the bomb used). c) Basaltic bomb field from Pampas Negras at the PY-4 location, Los Volcanes, PVF. d) Basaltic bombs (PY-7) from the Santa Maria volcano, PVF (circle indicates the bomb used). e) Basaltic lava flow (PY-8) from Santa Maria volcano, PVF. f) Ropy basaltic lava flow (PY-9), PVF; camera lens cover for scale 7.0 cm (circle indicates the sampling site).

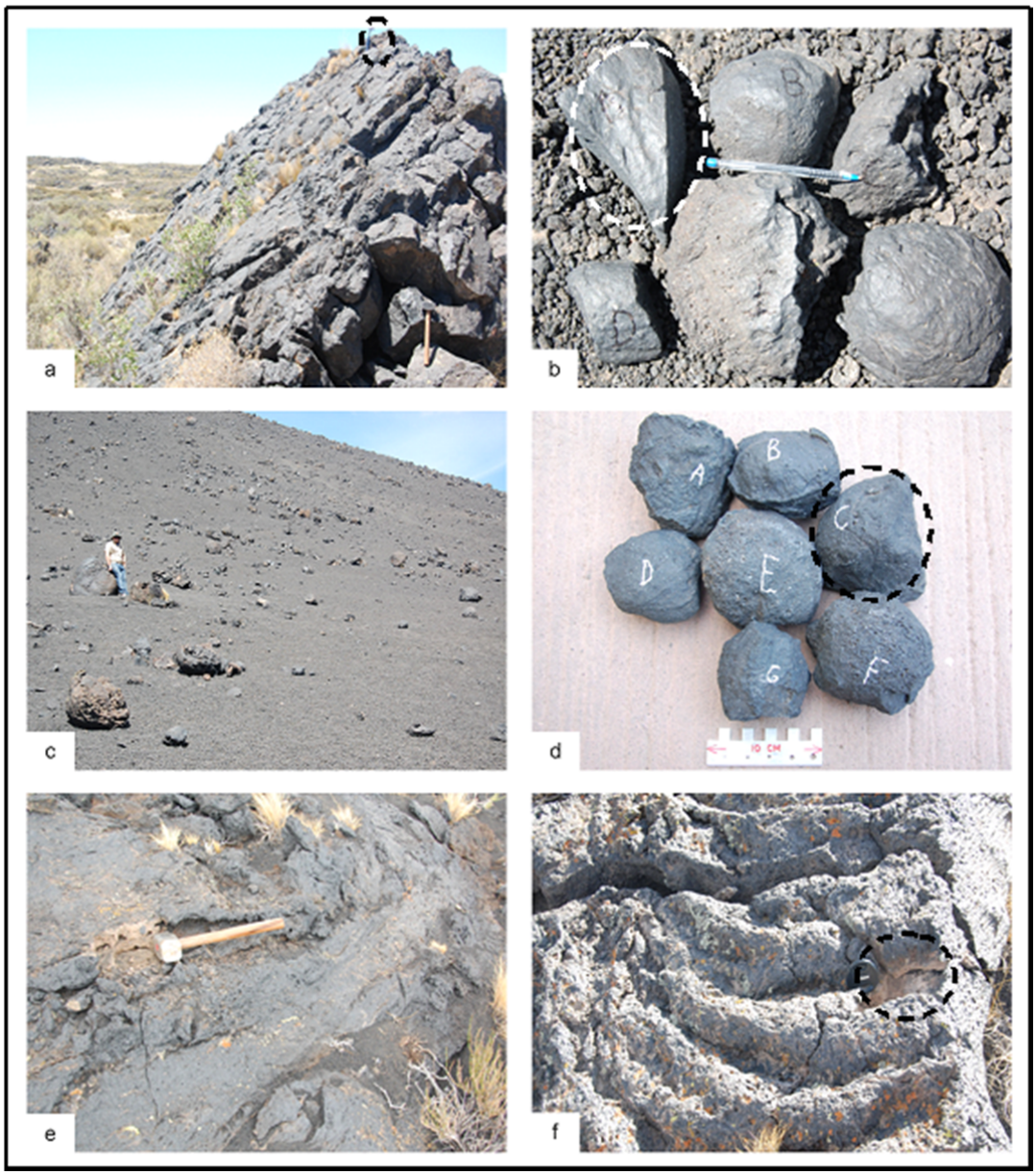

Fig 3: Total neon three-isotope diagram ($^{22}Ne/^{20}Ne$ vs $^{21}Ne/^{20}Ne$) of samples from Llancanelo (LL) and Payunia (PY) Volcanic Fields. The atmospheric neon composition is shown as "AIR". The cosmogenic line indicating mixtures of atmospheric and cosmogenic Ne is from Schäfer et al. (1999). The crustal neon line is from Kennedy et al. (1990) and the MORB neon component is from Sarda et al. (1988). The mass-fractionation line (mfl) for atmospheric Ne is shown in the diagram. The minimum Ne isotope composition expected to be seen in a diffusive phase by single-stage mass fractionation (cf. Matsumoto et al., 2004) is marked as a black square in the diagram. Note that the Ne isotope compositions observed in samples PY-7 and PY-8 are atmospheric within uncertainties.

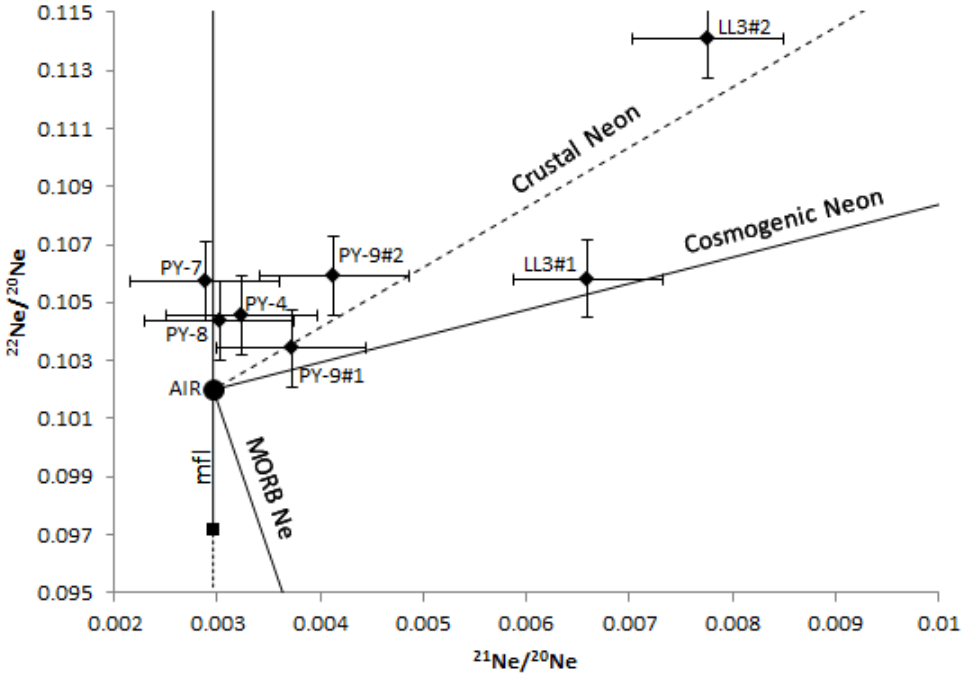

Fig 4: Plot of cosmogenic 3He vs 21Ne ages with 1σ uncertainties, in relation to the 1:1 line. Note that all samples fall on the right hand side of the 1:1 line.

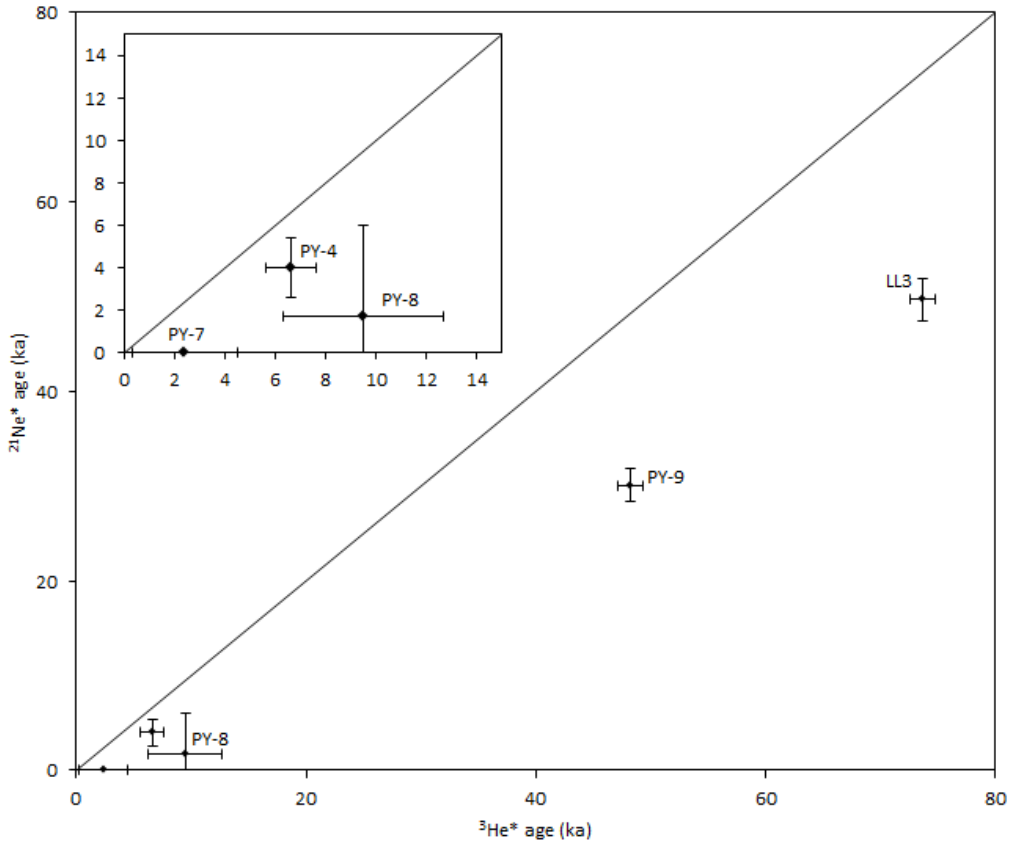

Fig 5: Map of the Payunia Volcanic Field (PVF) showing the ages obtained from this study (white crosses) from ^{3}He* (upper age in white rectangle) and ^{21}Ne* (lower age in white rectangle) with ages from Marchetti et al. (2013) (black crosses) and a K-Ar age from Germa et al. (2010) (sample 94AF; grey cross). The Holocene distribution of the flows, scoria field and cones is from Hernando et al. (2012) and the background is from the hill-shaded ASTER Global Digital Elevation Model, GDEM V1 (www.jspacesystems.or.jp/ersdac/GDEM/E/index.html).

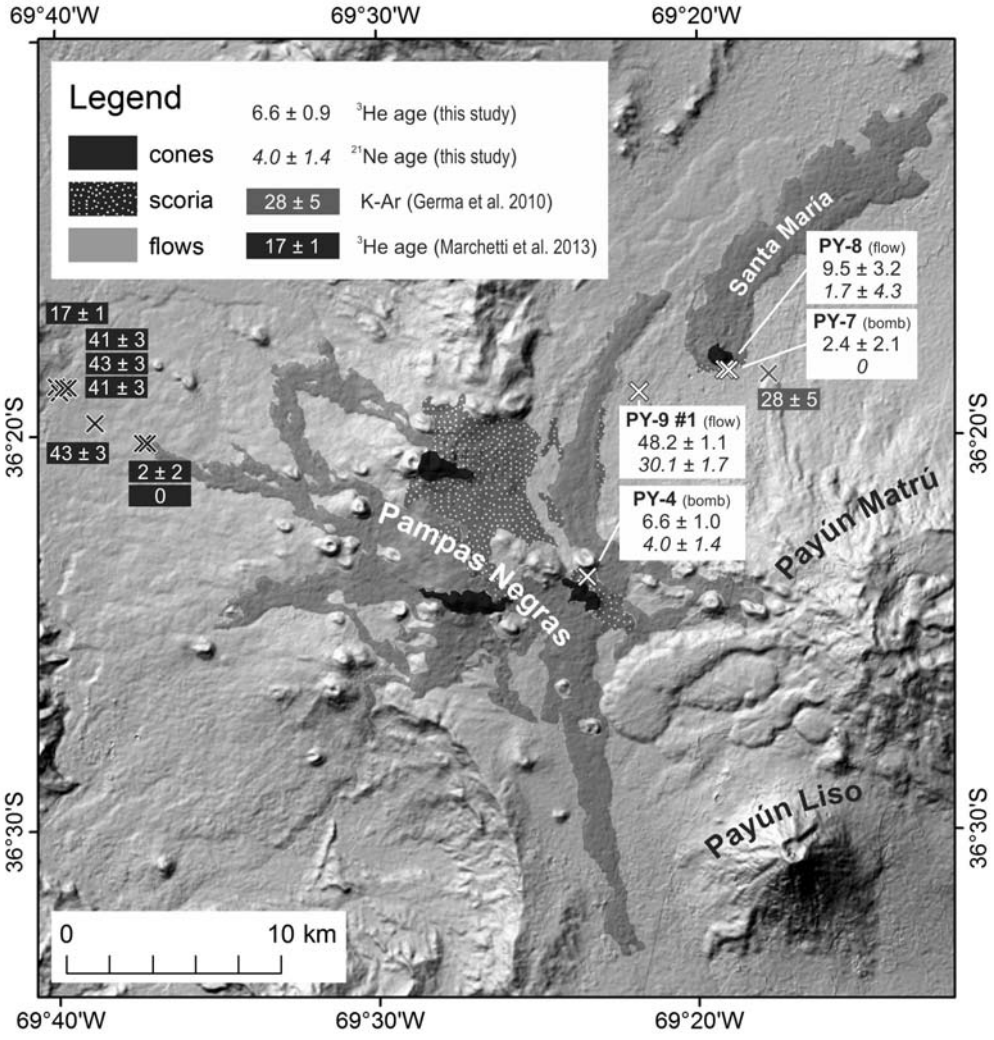

Table Captions

Table 1: Sample description and location of each sampling site from the Llancanelo (LLVF) and Payunia Volcanic (PVF) Fields.

Table 1

Sample name	Location	Latitude S	Longitude W	Elevation (m)	CosmoCalc Lal (1991) scaling factor[a]
LL3	Basaltic tumulus from LLVF	35.71184°	69.45692°	1449	2.817
PY-4	Basaltic bomb, Pampas Negras, PVF	36.39371°	69.39119°	2301	5.164
PY-7	Basaltic bomb, Santa Maria volcano, PVF	36.30600°	69.31853°	1811	3.696
PY-8	Basaltic flow, Santa Maria volcano, PVF	36.30600°	69.31853°	1811	3.696
PY-9	Basaltic flow, 3.8 km SW of Santa Maria, PVF	36.31536°	69.36352°	1907	3.952

Geographical coordinates WG84 datum

[a] CosmoCalc (https://sites.google.com/site/cosmocalc/) Vermeesch, 2007.

Table 2: Major-element XRF analysis of olivine separates.

Table 2

Wt (%)	LL3	PY-4	PY-7	PY-8	PY-9
SiO_2	39.23	41.52	39.50	40.79	41.19
TiO_2	0.11	0.43	0.19	0.52	0.56
Al_2O_3	1.72	1.98	1.22	2.49	2.14
ΣFeO	20.73	15.48	16.52	15.75	18.89
MnO	0.29	0.22	0.23	0.22	0.29
MgO	36.64	37.04	39.11	34.59	31.65
CaO	1.20	4.46	1.84	4.54	5.43
Na_2O	0.31	0.22	0.19	0.49	0.39
K_2O	0.04	0.05	0.06	0.14	0.09
P_2O_5	0.02	0.03	0.03	0.05	0.07
total	100.29	101.42	98.89	99.59	100.69
Fo[a]	76	81	81	80	75

[a] forsterite content (atomic Mg/(Mg+Fe) of olivine separates calculated from Mg and Fe contents.

Table 3: Helium and neon isotopic compositions obtained by stepwise heating at various temperatures for samples from the Llancanelo and Payunia Volcanic Fields.

Table 3

Sample name	Grain size (μm)	Temperature (°C)	^{4}He (10^{-9})[a]	^{20}Ne (10^{-11})[a]	$^{3}He/^{4}He$ (10^{-5})	$^{21}Ne/^{20}Ne$ (10^{-3})	$^{22}Ne/^{20}Ne$ (10^{-1})
LL3#1 (3.274 g)	180 -106	900	9.876 ± 0.043	4.68 ± 0.12	10.61 ± 0.12	3.601 ± 0.079	1.0271 ± 0.0060
		1400	4.585 ± 0.023	0.726 ± 0.020	3.29 ± 0.22	27.84 ± 0.59	1.286 ± 0.014
		1750		0.63 ± 0.057		4.403 ± 0.42	1.026 ± 0.022
		total	14.462 ± 0.049	6.04 ± 0.14	8.28 ± 0.11	6.60 ± 0.14	1.0582 ± 0.0056
LL3#2 (0.953 g)	355-180	900	2.204 ± 0.032	4.47 ± 0.34	39.3 ± 1.0	3.26 ± 0.19	1.096 ± 0.011
		1750	2.310 ± 0.030	1.592 ± 0.074	14.8 ± 1.2	20.41 ± 0.77	1.266 ± 0.029
		total	4.513 ± 0.044	6.06 ± 0.35	26.78 ± 0.77	7.76 ± 0.38	1.141 ± 0.012
PY-4 (1.541 g)	355-180	900	6.659 ± 0.029	11.08 ± 0.21	1.73 ± 0.14	3.095 ± 0.044	1.0397 ± 0.0073
		1750	32.47 ± 0.12	1.36 ± 0.17	1.357 ± 0.059	4.39 ± 0.47	1.092 ± 0.041
		total	39.13 ± 0.12	12.45 ± 0.28	1.421 ± 0.055	3.237 ± 0.067	1.0454 ± 0.0079
PY-7 (1.007 g)	355-106	900	8.756 ± 0.041	9.17 ± 0.31	1.41 ± 0.25	2.814 ± 0.072	1.0286 ± 0.0071
		1750	15.094 ± 0.063	1.42 ± 0.14	1.07 ± 0.19	3.30 ± 0.34	1.244 ± 0.048
		total	23.850 ± 0.075	10.58 ± 0.34	1.19 ± 0.15	2.879 ± 0.078	1.0574 ± 0.0092
PY-8 (0.264 g)	355-180	1750	25.85 ± 0.23	15.54 ± 0.94	1.65 ± 0.21	3.02 ± 0.17	1.044 ± 0.015
PY-9#1 (3.026 g)	180 -106	900	12.216 ± 0.055	22.89 ± 0.29	6.81 ± 0.10	3.014 ± 0.029	1.0225 ± 0.0054
		1400	19.315 ± 0.084	1.050 ± 0.032	1.885 ± 0.055	18.30 ± 0.41	1.238 ± 0.014
		1750	2.875 ± 0.018	0.253 ± 0.052	1.78 ± 0.29	7.0 ± 1.3	1.251 ± 0.046
		total	34.35 ± 0.10	24.19 ± 0.28	3.619 ± 0.054	3.712 ± 0.042	1.0342 ± 0.0052
PY-9#2 (1.091 g)	355-106	900	19.281 ± 0.074	11.28 ± 0.40	3.90 ± 0.12	3.046 ± 0.080	1.0549 ± 0.0068
		1750	25.76 ± 0.10	4.15 ± 0.33	1.111 ± 0.068	7.10 ± 0.41	1.071 ± 0.016
		total	45.04 ± 0.12	15.43 ± 0.52	2.303 ± 0.064	4.14 ± 0.14	1.0592 ± 0.0066
AIR					0.138	2.959	1.020

[a] gas abundance expressed in cm^3 STP/g.

Note: #1 and #2 represents aliquot 1 and 2 for samples LL3 and PY-9.

Table 4: Cosmogenic 3He and 21Ne concentrations, production rates and corresponding ages.

Table 4

Sample name	Th (ppm) whole rock	U (ppm) whole rock	Li (ppm) whole rock	Th (ppm) olivine sep.	U (ppm) olivine sep.	Li (ppm) olivine sep.	predicted radiogenic ^{4}He (10^5 at g^{-1})[a]	total measured ^{4}He (10^5at g^{-1})[b]	% of radiogenic ^{4}He in sample	predicted nucleogenic ^{3}He (at g^{-1})[c]	Nucleogenic ^{21}Ne (at g^{-1})[d]
LL3#1	1.98	0.469	6.33	0.063	0.021	16.0	43	388	11	140	2129
LL3#2	1.98	0.469	6.33	0.063	0.021	16.0	43	121	35	140	2129
PY-4	2.36	0.691	5.28	0.10	0.025	1.77	1.9	1050	0.18	1.3	95
PY-7	5.72	1.25	7.40	0.18	0.044	1.62	1.8	639	0.28	2.1	91
PY-8	8.82	1.20	7.40	0.42	0.11	2.74	15	682	2.2	12	762
PY-9#1	5.82	0.714	4.03	0.20	0.057	2.97	33	822	3.6	33	1677
PY-9#2	5.82	0.714	4.03	0.20	0.057	2.97	33	1186	2.8	33	1677

[a] Radiogenic ^{4}He calculated from U and Th concentration of the olivine separate and whole rock based on the equations of Blard and Farley (2008).

[b] Total measured ^{4}He.

[c] Nucleogenic ^{3}He calculated from Li, U and Th concentration using a maximum age of 100 ka for sample LL3, 50 ka for PY-9, 10 ka for PY-8 and 7 ka for PY-4 and PY-7; based on the equations of Andrews (1985).

[d] Nucleogenic ^{21}Ne calculated using the radiogenic ^{4}He and the reported ratio of $^{21}Ne_{nucleogenic}$/ $^4He_{radiogenic}$ of 5x10^{-8} from Yatsevich and Honda (1997).

Table 5: Predicted nucleogenic 3He, radiogenic 4He, nucleogenic 21Ne and concentration of U, Th and Li from olivine separates.

Table 5

Sample name	^{3}He* (10^6 at g^{-1})	^{21}Ne* (10^6 at g^{-1})	^{21}Ne*/^{3}He*	P^{3}He [a]	P^{21}Ne [b]	P^{21}Ne/P^{3}He	^{3}He age (ka)	^{21}Ne age (ka)
LL3#1	25.11 ± 0.39	5.91 ± 0.26	0.235 ± 0.011	341	119	0.349	73.7 ± 1.1	49.7 ± 2.2
PY-4	4.13 ± 0.63	0.93 ± 0.22	0.226 ± 0.064	625	232	0.372	6.6 ± 1.0	4.0 ± 1.4
PY-7	1.07 ± 0.97	0	0	447	166	0.372	2.4 ± 2.12	-
PY-8	4.26 ± 1.4	0.27 ± 0.71	0.064 ± 0.168	447	164	0.367	9.5 ± 3.2	1.7 ± 4.3
PY-9#1	23.06 ± 0.54	4.95 ± 0.28	0.214 ± 0.013	478	164	0.344	48.2 ± 1.1	30.1 ± 1.7

[a] Production rate in at g^{-1} a^{-1} calculated according to local latitude and altitude using Lal's scaling factor and using the Goehring et al., 2010 production rate of 121 ± 11 at g^{-1} a^{-1}.

[b] Production rate in at g^{-1} a^{-1} calculated according to local latitude and altitude using Lal's scaling factor and the Poreda and Cerling, 1992 production rate of 45 ± 4 at g^{-1} a^{-1}.